

Mesomorphic and structural properties of liquid crystal possessing a chiral lactate unit

Banani Das^a, Anamika Pramanik^b, Malay Kumar Das^{b,*}, Alexej Bubnov^c, Věra Hamplová^c, Miroslav Kašpar^c

^a Department of Physics, Siliguri Institute of Technology, Siliguri, Darjeeling 734 009, West Bengal, India

^b Department of Physics, University of North Bengal, Siliguri, Darjeeling 734 013, West Bengal, India

^c Institute of Physics, Academy of Sciences of the Czech Republic, Na Slovance 2, 18221 Prague, Czech Republic

ARTICLE INFO

Article history:

Received 28 October 2011

Received in revised form 15 January 2012

Accepted 17 January 2012

Available online 28 January 2012

Keywords:

Liquid crystals

Phase transition

TGB_A phase

X-ray diffraction

Differential scanning calorimetry

Dielectric properties

ABSTRACT

The mesomorphic and structural properties of the chiral lactic acid derivative 4'-(1-(octyloxy)-1-oxopropan-2-yloxy) biphenyl-4-yl 4-(decyloxy)benzoate have been studied. The compound shows the blue phase (BPII), the cholesteric (N^{*}), the TGB_A and the paraelectric SmA^{*} phases over a broad temperature range. Polarising optical microscopy, differential scanning calorimetry, optical transmission, X-ray diffraction and dielectric spectroscopy studies have been performed. In the SmA^{*} phase the layer spacing (*d*) values are found to be slightly temperature dependent and suggest that there is no bi-layer association present in the mesophase. In the TGB_A phase, the *d* values show strong temperature dependence near SmA^{*}–TGB_A phase transition, indicating pre-transitional effect. The temperature dependence of scattered X-ray intensities indicate the appearance of long range smectic ordering at the N^{*}–TGB_A phase transition. Near the TGB_A–SmA^{*} phase boundary strong SmA^{*} fluctuations predominate. This behaviour is also observed from the temperature dependence of the *d* values. The transverse correlation lengths, ξ_{\perp} , diverge near the N^{*}–TGB_A phase transition indicating second order phase transition.

© 2012 Elsevier B.V. All rights reserved.

1. Introduction

Liquid crystalline (LC) materials exhibiting a great variety of structures are strongly susceptible to external fields as well as surface interactions, and provide multiple functionality. Thermodynamically liquid crystalline materials are located between the three-dimensionally ordered solid state (crystal) and the isotropic liquid. For particular molecules assembled in specific architectures, permanent dipole moment can appear thus forming structures with a polar order, namely paraelectric, ferroelectric or antiferroelectric phases [1]. Such materials can be utilised as a self-assembling media combining the necessary order and fluidity on a molecular (nano-scale) level [2,3].

While designing chiral liquid crystalline materials, the type of chiral fragment used in the molecule plays a very important role in determining its mesomorphic behaviour. In 1988 Taniguchi et al. [4] synthesized and studied series of compounds with phenyl-4'-alkoxybiphenyl-4-carboxylate as a molecular core and one lactate group as a chiral centre. These compounds possess a broad range of the paraelectric smectic A^{*} (SmA^{*}) and ferroelectric smectic C^{*} (SmC^{*}) phases. During the last years, lactic acid derivatives

differing in number of the lactate groups as chiral centres have been attracting attention as they show a rich variety of the polar liquid crystalline mesophases [5–12]. Use of the lactic unit as a precursor of chiral centre have two advantages with respect to other types of chiral centres: (i) they minimise the cost, as the price ratio to the most commonly used chiral precursor material (*S*)-2-octanol is at least 1:100 and (ii) lactic acid-based LCs usually show no aging and are highly stable, thermally as well as chemically. Lactate based chiral moiety has provided many materials with a very rich variety of the liquid crystalline mesophases [13–19]. Several new liquid crystalline materials containing one, two or three chiral centres and having one or two lactate groups attached to the molecular core by the ether linkage group have been synthesized and studied [20,21].

However, several basic questions are still open, especially those concerning the interactions between the molecular core and aliphatic chains, relation between the chemical structure, mesophase behaviour and the physical properties of the polar mesophases. Therefore, the investigation of the structure–property relationship for lactic acid derivatives possessing liquid crystalline behaviour is still of great significance for further progress, both for the understanding of the basic properties as well as for their practical use in potential applications. The understanding of the mesophase nano-scale organisation will enable generalisation of relation

* Corresponding author. Tel.: +91 3532582605; fax: +91 3532699001.

E-mail address: mkdnbu@yahoo.com (M.K. Das).

between molecular structure and macroscopic properties of liquid crystalline materials. Molecules with pronounced features related to the macroscopic properties could then be synthesised.

In order to contribute towards better understanding of structure – property relationship, the mesomorphic and structural properties of the chiral lactic acid derivative, namely 4'-(1-(octyloxy)-1-oxopropan-2-yloxy) biphenyl-4-yl 4-(decyloxy)benzoate, possessing liquid crystalline behaviour have been studied by polarising optical microscopy, differential scanning calorimetry, optical transmission, X-ray diffraction and dielectric spectroscopy.

2. Experimental

2.1. Material under the study

General synthetic procedure for chiral lactic acid derivative is presented in Fig. 1. The synthesis started from 4-n-decyloxybenzoic acid. The compound on reaction with an excess of thionylchloride and 4,4'-biphenol yielded 4-(4'-hydroxybiphenyl)4-n-decyloxybenzoate. Optically active octyl lactate was prepared from commercial (S)-(+)-lactic acid by azeotropic esterification with octylalcohol. DEAD (diethyl azodicarboxylate) supported coupling in the presence of triphenylphosphine in tetrahydrofuran followed by column chromatography gave the final compound. However, the detailed synthetic procedure for the 4'-(1-(octyloxy)-1-oxopropan-2-yloxy) biphenyl-4-yl 4-(decyloxy)benzoate (material under the study) has been described in details in our earlier publication [20].

The raw product was purified by column chromatography on silicagel (Kieselgel 60) using a mixture of dichloromethane and ethanol (99:1) as an eluent. Recrystallization was made twice from ethanol producing white powder. The chemical purity of the material was checked by high pressure liquid chromatography (HPLC), which was carried out using a silica gel column (Bioshere Si 100-5 μm , 4×250 , Watrex) with a mixture of 99.9% of toluene and 0.1% of methanol as an eluent, and the eluting products were detected by a UV-VIS detector ($\lambda = 290 \text{ nm}$). The chemical purity of the synthesised compound was found to be 99.6% under these conditions.

Structures of the intermediates and the final liquid crystalline material were checked by the Nuclear Magnetic Resonance (NMR) spectroscopy. A 300 MHz Varian spectrometer with tetramethylsilane as internal standard was used for ^1H and ^{13}C NMR studies.

^1H NMR of 4-(4'-hydroxybiphenyl)4-n-decyloxybenzoate (300 MHz, CDCl_3): 8.16 (d, 2H, ortho to $-\text{COO}$); 7.55 and 7.43

(dd, 4H, ortho to $-\text{Ar}$); 7.23 (d, 2H, ortho to $-\text{OCO}-$); 6.99 (d, 2H, ortho to $-\text{OCH}_2$); 6.87 (d, 2H, ortho to $-\text{OH}$); 5.00 (brs, 1H, OH); 4.05 (t, 2H, CH_2O); 1.20–1.80 (m, 16H, CH_2); 0.90 (t, 3H, CH_3).

^1H NMR of final product (300 MHz, CDCl_3): 8.15 (d, 2H, ortho to $-\text{COO}$); 7.56 and 7.50 (dd, 4H, ortho to $-\text{Ar}$); 7.24 (d, 2H, ortho to $-\text{OCO}-$); 6.96 (dd, 4H, ortho to $-\text{O}$); 4.80 (q, 1H, CH^*); 4.17 (m, 2H, COOCH_2); 4.03 (t, 2H, CH_2OAr); 1.80 (m, 4H, $\text{CH}_2\text{CH}_2\text{O}$); 1.62 (d, 3H, CH_3C^*); 1.20–1.60 (m, 24H, CH_2); 0.87 (m, 6H, CH_3).

Chemical formula of the final product indicating the carbon atom numbers and the chemical shift (δ) obtained from ^{13}C NMR spectroscopy (300 MHz, CDCl_3) are presented in Table 1.

2.2. Mesomorphic properties

The sequence of phases and phase transition temperatures were identified by observing the textures and their changes under the polarising optical microscope. The LINKAM LTS E350 heating stage with TMS-93 temperature programmer was used for temperature control, which enabled temperature stabilisation within $\pm 0.1 \text{ K}$. In addition, free – standing films were also prepared, in which the liquid crystalline material was mechanically spread over a circular hole (diameter 3 mm) in a metallic plate. The phase transition temperatures were checked by Differential Scanning Calorimetry (Pyris Diamond Perkin-Elmer 7) on cooling/heating runs at a rate of 5 K min^{-1} in a nitrogen atmosphere. The sample (5 mg) was hermetically sealed in an aluminium pan and placed in a nitrogen atmosphere. The temperature was calibrated on extrapolated onsets of the melting points of water, indium and zinc. The enthalpy change [ΔH] was calibrated on enthalpies of melting of water, indium and zinc.

2.3. Optical transmission

Optical transmission method [22] on samples with planar and homeotropic alignment was also used for identification of the liquid crystalline phases. A linearly polarised He-Ne laser beam ($\lambda = 632.8 \text{ nm}$) was used as a light source and directed onto a homogeneously (or homeotropically) aligned Indium Tin Oxide (ITO) coated liquid crystalline cell (purchased from AWAT Co. Ltd., Warsaw, Poland) placed between two crossed linear polarizers. The temperature of the cell in a brass thermostat was controlled by Eurotherm PID 2216e temperature controller, which enabled temperature stabilisation within $\pm 0.2 \text{ K}$. The light transmittance was measured by a photodiode detector and recorded

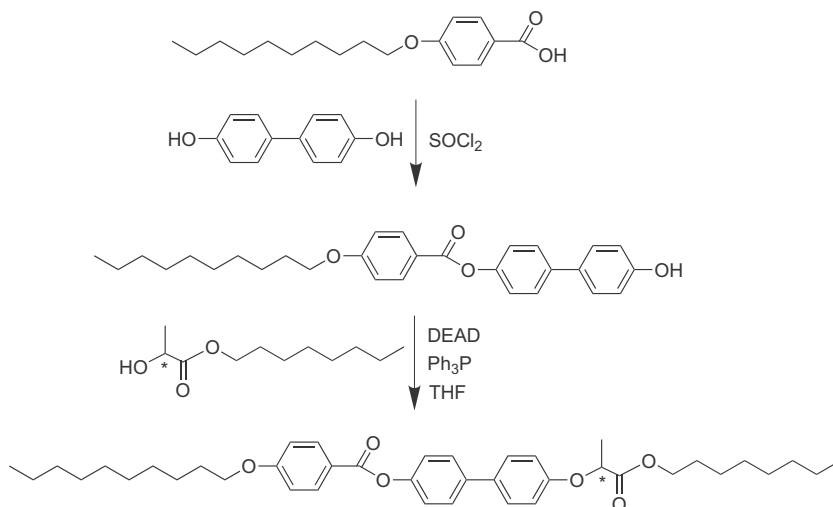
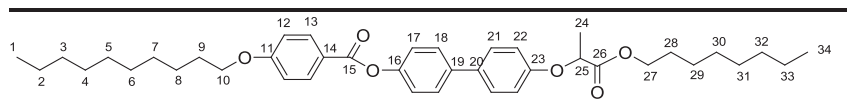


Fig. 1. Schematic illustration of synthetic procedure for 4'-(1-(octyloxy)-1-oxopropan-2-yloxy) biphenyl-4-yl 4-(decyloxy)benzoate.

Table 1
Chemical shift δ (ppm) for 4'-(1-(octyloxy)-1-oxopropan-2-yloxy)biphenyl-4-yl 4-(decyloxy)benzoate from ^{13}C NMR.



Carbon no.	δ (ppm)	Carbon no.	δ (ppm)
1	14.27	19	138.51
10	68.57	20	134.12
11	157.46	21	127.95
12	114.54	22	115.60
13	132.50	23	163.80
14	121.81	24	18.83
15	165.21	25	72.97
16	150.40	26	172.47
17	122.22	27	65.65
18	128.42	34	14.31

digitally by a Keithley 2000 multimeter. The transmitted light intensity was measured as a function of temperature. From the temperature dependence of the transmitted light intensity, we could identify the phase transition temperatures, especially those transitions, which could not be detected by DSC. Such method has been successfully used in our investigations of other liquid crystalline molecules like hockey-stick shaped mesogens [23,24].

2.4. Dielectric spectroscopy

The temperature dependence of the real part of complex permittivity ($\epsilon' = \epsilon' - i\epsilon''$) was measured on cooling using a Schlumberger 1260 impedance analyzer at a frequency of 160 Hz. Planar sample of thickness 12 μm was used for dielectric spectroscopy measurement.

2.5. X-ray diffraction

X-ray diffraction measurements were done on the samples filled into Mark capillary tubes of 0.7 mm diameter, in the presence of a magnetic field (1 T). The temperature of the sample was regulated by a temperature controlled heating stage. The X-ray patterns were recorded on a 2D area detector (HI – Star, Siemens AG) using Ni-filtered Cu K α radiation (wavelength $\lambda = 1.5418 \text{ \AA}$). From the X-ray diffraction studies the smectic layer spacing (d) in the TGB_A and SmA* phases (or apparent molecular length (l) in the case of blue phase and the cholesteric (N*) phase) and the average intermolecular distance between the long axes of neighbouring parallel molecules (D) were calculated from the position of the small angle ($\theta = 0.2\text{--}4.5^\circ$) and wide angle diffraction peaks, respectively for all the phases.

The MOPAC/AM1 model was used to ascertain the length of LC molecules corresponding to the state with minimum energy. In Fig. 2, picture of molecule with the axis corresponding to the smallest principal moment of inertia is presented. Taking into account the most extended conformer (length of the molecule in the direction of the long molecular axis), the length of molecule is calculated to be 43 \AA .

3. Results and discussion

3.1. Texture and DSC studies

The phase sequences of the materials were determined from characteristic textures and their changes observed under a polarising optical microscope. Phase transition temperatures have been

checked and the related enthalpies have been measured using DSC. The respective thermogram on heating and cooling runs is presented in Fig. 3. Phase transition temperatures are shown in Table 2. On cooling from the isotropic (Iso) phase the studied LC material exhibited the blue phase (BPII), the cholesteric phase, the twist grain boundary smectic A (TGB_A) phase and the paraelectric SmA* phase.

In Fig. 4, several characteristic microphotographs of the mesophase textures of the sample in planar alignment (a–e) and free standing film (f) are presented. In particular, a very characteristic platelet texture of the blue phase (Fig. 4a), oily streaks texture of the cholesteric phase (Fig. 4c) and filament texture of the TGB_A–SmA* phase transition (Fig. 4f) helped to unambiguously detect the type of mesophases. Due to quite low enthalpies of the Iso–BPII, N*–TGB_A and TGB_A–SmA* phase transitions, the respective transitions were hardly detectable by DSC but were well defined by polarising optical microscopy. Again, the optical transmission studies were quite helpful for the identification of some of the phase transitions which were not clearly detected from DSC measurements.

3.2. Optical transmission study

Fig. 5 shows the temperature dependence of the transmitted intensity from planar as well as on homeotropic cells (8.9 μm thickness) placed between two crossed linear polarizers. Interestingly, the N*–TGB_A and TGB_A–SmA* phase transition temperatures, which were not clearly detectable from DSC measurements, could be identified clearly. However, the Iso–BPII, BPII–N* phase transitions, which were visible in DSC measurement (Fig. 3) were not clearly identifiable in the optical transmission method. Hence, the conclusion regarding the existence of the different mesophases is based on observations from all the three used methods, namely the study of textures and their changes under polarising optical microscope, DSC runs and optical transmission studies.

3.3. X-ray diffraction

Fig. 6(a–c) shows the X-ray diffraction photographs of the unaligned sample obtained in the BPII, TGB_A and SmA* phases at 86 $^\circ\text{C}$, 70 $^\circ\text{C}$ and 50 $^\circ\text{C}$ respectively. From the X-ray diffraction patterns it is clear that it was not possible to align the compound with a magnetic field of about 1 T. The pattern obtained immediately below the clearing temperature (Fig. 6a) i.e. in the BPII show the presence of diffuse rings both in the small and wide angle regions typical for the non-oriented samples. The absence of sharp inner ring

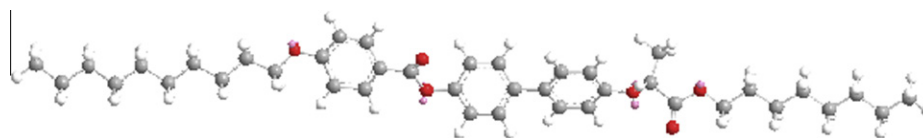


Fig. 2. Conformation of the molecule after energy minimisation using MOPAC/AM1 method.

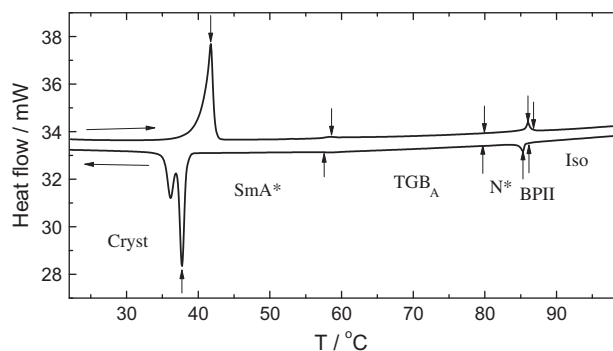


Fig. 3. DSC thermograms on heating and cooling cycles taken at a rate 5 K min^{-1} . Vertical arrows indicate the Iso-BPII, BPII-N*, N*-TGB_A and TGB_A-SmA* phase transitions subsequently on heating (→) and cooling (←).

indicates that this mesophase is rather fluid like. We have also obtained a similar pattern in the N* phase which is expected. Below 78°C we observe relatively sharp inner ring and a diffuse outer ring in the X-ray diffraction pattern (Fig. 6b) and the intensity of the inner ring increases with decreasing temperature. The pattern represents the unoriented TGB_A phase as observed from polarising optical microscopy. The intense peak in the small angle region corresponds to the smectic layer thickness in the TGB_A phase. On further cooling (Fig. 6c) the outer diffraction pattern remains the same but the inner ring becomes distinctly sharper and hence this pattern suggests the appearance of the non-oriented SmA* phase.

Fig. 7 shows the X-ray diffraction intensity profiles obtained from a linear scan of the diffraction patterns of the non-oriented sample in different mesophases. The intensity profile reveals the presence of relatively sharp reflections at small angles ($2\theta \approx 3\text{--}4^\circ$) in the TGB_A and SmA* phase, clearly indicating the layered structure, in comparison to the diffuse ring obtained in the case of the BPII and N* phases. The diffuse outer scattering at wide angles ($2\theta \approx 18\text{--}24^\circ$) corresponds to the average intermolecular distance D between the long axes of neighbouring parallel molecules.

The values of the effective molecular length (l) in case of the BPII and N* phases and the smectic layer thickness (d) in the TGB_A and SmA* phases as well as the intermolecular distance between the long axes of the neighbouring molecules D , at different temperatures were determined. The temperature dependence of the l or d values and intermolecular distance D are presented in Figs. 8 and 9 respectively. Interestingly, the layer spacing of the SmA* phase is found to have a slight temperature dependence with the d values changing from 37.5 \AA at the TGB_A-SmA* phase transition to 39 \AA within the phase. The increase in layer spacing values of the SmA* phase on cooling is perhaps due to stretching of the aliphatic chains of the molecule. Within the temperature range of the TGB_A

phase (the type of the mesophase has been determined from typical textures obtained on free standing films), the d values initially increase slowly (31.7 \AA) with decrease in temperature. However, we observe a rapid increase in d (37.7 \AA) as the TGB_A-SmA* phase transition is approached. In fact, its value coincides with the SmA* layer spacing. Thus within the TGB_A phase, the ratio $d/l \sim 0.74\text{--}0.88$ which is typical of monolayers and also is a signature of the SmA nature of the blocks of the TGB_A phase. The effective molecular length (l) in case of the BPII and N* phases increases with decrease in temperature. The increase in l values in going from the N* to TGB_A phase has also been reported by Shankar Rao et al. [25]. The intermolecular distance, i.e. the average lateral distance between the long axes of molecules, D , decreases with decrease in temperature, as expected.

The temperature dependence of the intensity of the inner ring (with nearly same exposure time) is presented in Fig. 10. It is observed that the X-ray intensity is nearly constant in the N* phase. However, the intensity values appear to show a discontinuous increase at the transition from N* to TGB_A phase. Within the TGB_A phase the X-ray intensity increases with decrease in temperature and this increase is quite rapid as the TGB_A-SmA* phase transition is approached. It may be mentioned here, that, the reason for the appearance of the TGB_A phase is that a direct cholesteric-smectic phase transition cannot occur in a continuous way since the cholesteric twist of the director is not compatible with the smectic layering. Thus we observe a definite increase in the scattered X-ray intensities at the onset of the TGB_A phase at the N*-TGB_A phase boundary signifying the appearance of long range order in layering within this phase. Again, as observed from Fig. 10, there is a significant increase in the intensity values near the TGB_A-SmA* phase transition. SmA* fluctuations dominate in this region as the twist of the smectic blocks within the TGB_A phase gradually unwinds and smectic A like ordering appears. This behaviour again verifies the existence of the TGB_A phase. Similar behaviour is also observed in the d values as mentioned in the previous paragraph.

The longitudinal (ξ_{\parallel}) as well as the transverse in-plane (ξ_{\perp}) correlation length in different mesophases have been determined from a linear scan of the inner and outer diffraction peaks. The intensity profile $I(q)$ was then fitted to a Lorentzian form with a quadratic background viz.,

$$I(q) = \frac{a_1}{a_2 + (q - q_0)^2} + a_3q^2 + a_4q + a_5 \quad (1)$$

where q is the magnitude of the scattering vector. Here a_1, a_2, q_0, a_3, a_4 and a_5 are the fitting parameters, which were adjusted to obtain the best fit. The transverse correlation length is defined as $\xi = 2\pi(a_2)^{-1/2}$. Fig. 11 shows the results for ξ_{\perp} and ξ_{\parallel} over the relevant temperature region. As expected, the correlation lengths for

Table 2
Sequence of phases, phase transition temperatures ($^\circ\text{C}$), transition enthalpies [ΔH (J/g)] (measured on cooling with DSC (5 K min^{-1})) and melting point m.p. ($^\circ\text{C}$) (measured on heating) for the studied compound. ("●" the phase exists).

m.p.	Cr	SmA*	TGB _A	N*	BPII	Iso
41.7 [+24.06]	●	●	●	●	●	●
	37.8 [-23.87]	58.5 [-0.33]	79.8 [-0.01]	85.3 [-0.96]	86.1 [-0.01]	

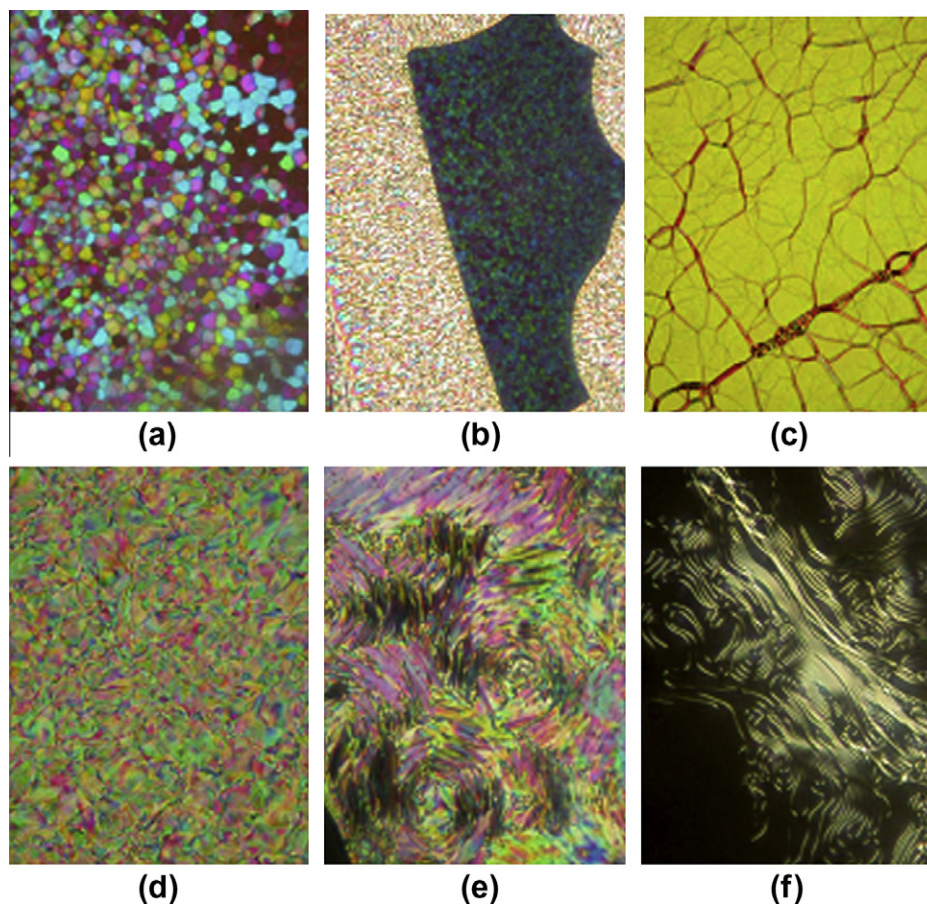


Fig. 4. Microphotographs of textures observed under the polarising optical microscope: (a) platelet texture of the blue phase (BPII) at 85.5 °C; (b) the BPII–N* phase transition at 85 °C; (c) the oily streaks texture of the cholesteric phase (N*) at 83 °C; (d) the texture of the TGB_A phase at 75 °C; (e) the TGB_A–SmA* phase transition at 58 °C; (f) the filament texture of the TGB_A–SmA* phase transition at 58 °C (free standing film). The width of all the photos is about 350 μm.

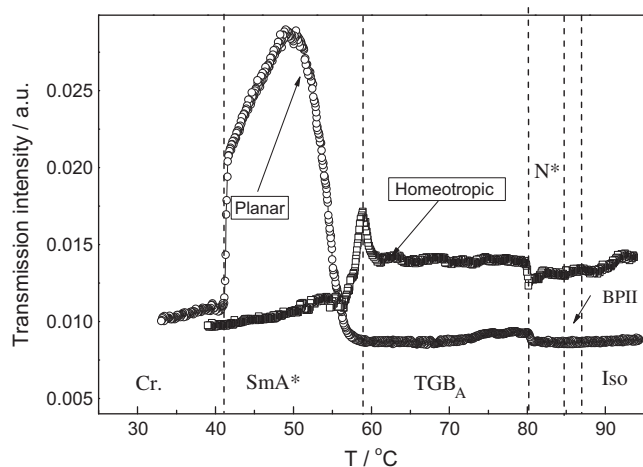


Fig. 5. Temperature dependence of the transmitted intensity obtained on samples in planar alignment (open circles) and homeotropic alignment (open squares).

the higher ordered phase are found to be much higher than those for the lower ordered phases.

The values of the transverse correlation lengths is about 50 Å in SmA* phase. In the vicinity of the SmA*–TGB_A phase transition, there is a rapid decrease of correlation length on heating from the SmA* phase to the TGB_A phase. At the TGB_A–N* phase transition there appears to be a divergence of ξ_{\perp} near the TGB_A–N* phase

transition point, as expected for a second order phase transition. These observations have also been supported by enthalpy and optical transmission measurements. The longitudinal correlation length, ξ_{\parallel} , increases rapidly at the N*–TGB_A phase transition from about 125 Å to nearly 325 Å near the TGB_A–SmA* phase transition. This rise continues even in the SmA* phase and reaches a value of about 350 Å at saturation. It is necessary to mention that for all studied phases, the correlation lengths are expected to be much longer. Possible explanation for this discrepancy may be due to the use of Ni filtered Cu K α radiation, which contains a white background radiation in addition to the Cu K α peak. No correction for this white radiation, which broadens the diffraction peaks considerably, is made here. Hence the experimental values of correlation lengths as obtained above are somewhat smaller than the theoretically expected values.

3.4. Dielectric spectroscopy

Temperature dependence of the real part of complex permittivity measured on cooling at a frequency of 160 Hz within the range of all detected mesophases is shown in Fig. 12. As no polar phase was detected for this chiral LC material, the only contribution of the soft mode in the paraelectric SmA* phase could be detected. It results in a pronounced increase of the real part of complex permittivity on cooling below the TGB_A–SmA* phase transition. A peak at the low temperature border of the SmA* phase is related to pre-crystallisation phenomena.

In order to study the effect of the molecular structure on mesomorphic properties, the compound studied in this work has been

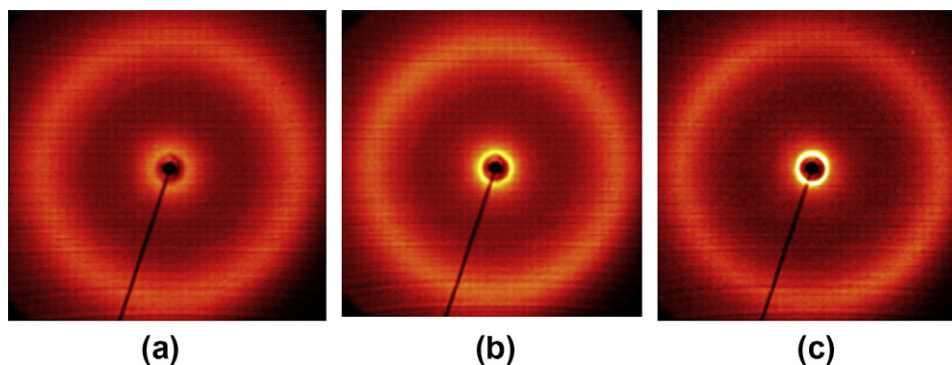


Fig. 6. X-ray diffraction photographs obtained on the unaligned sample in (a) BPII phase (85.5 °C); (b) TGB_A phase (70 °C) and (c) SmA* phase (50 °C).

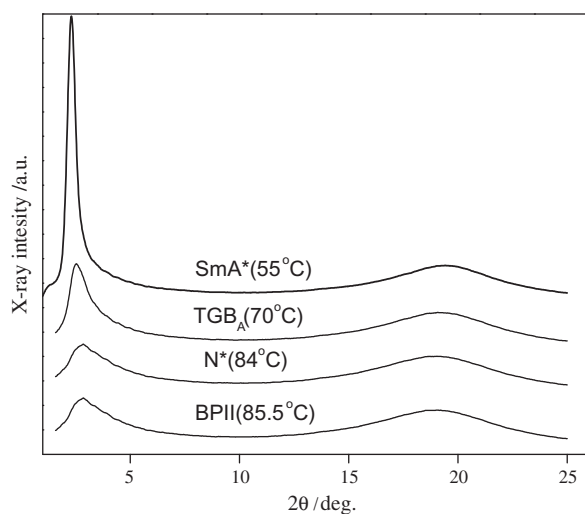


Fig. 7. X-ray diffraction profiles at indicated temperatures with nearly equal exposure time.

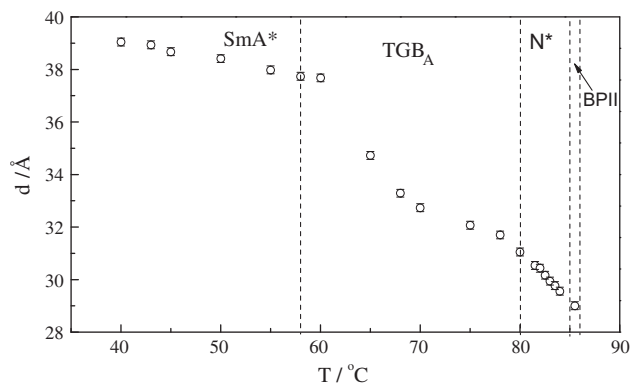


Fig. 8. Temperature dependence of the layer thickness d .

compared with compounds having slightly different molecular structure. In particular the effect of: (i) the influence of the chains length, (ii) lateral substitutions by various groups in different positions as well as (iii) the effect of the type of the group, which connect the chiral molecular chain, have been investigated. If the length of the non-chiral chain is increased, the tilted ferroelectric SmC* phase of about 20 K broad down to room temperature has been found [21]. The lateral substitution by two methyl groups [26] on the phenyl ring far from the chiral centre completely suppresses the mesomorphic properties. The same effect is reached

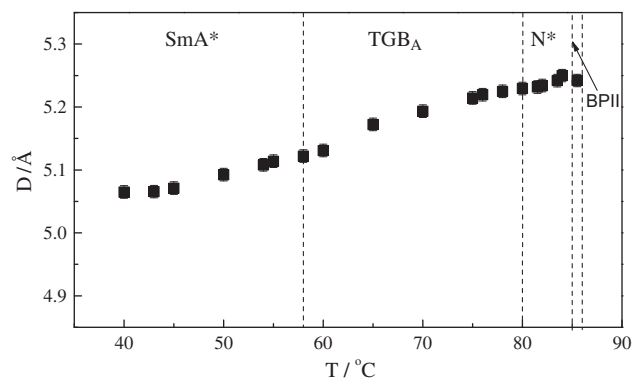


Fig. 9. Temperature dependence of the average intermolecular distance D .

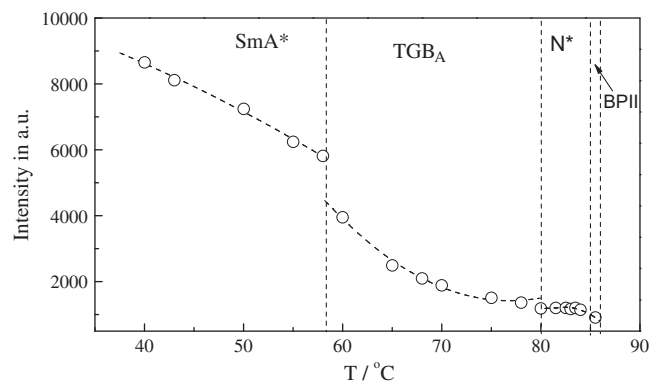


Fig. 10. Temperature dependence of the X-ray intensity of the inner ring (with nearly same exposure time).

by NO₂ group laterally substituted on phenyl ring close to the chiral centre [27]. In case of double lateral substitution, namely when the methyl group is placed far from the chiral centre and the NO₂ group is placed close to the chiral centre, no liquid crystalline behaviour can be detected [27]. However, the lateral substitution by the single methyl group on phenyl ring far from the chiral centre retains the cholesteric phase; the clearing point for that compound is about 40 K lower than that obtained for compound studied in the present work. Liquid crystalline material containing the chiral 2-alkoxypropionate unit (connected to the molecular core by ester group) instead of the chiral lactate unit (connected to the molecular core by ether group) possess a broad range of the cholesteric phase and the ferroelectric SmC* phase [28]. However, the clearing point

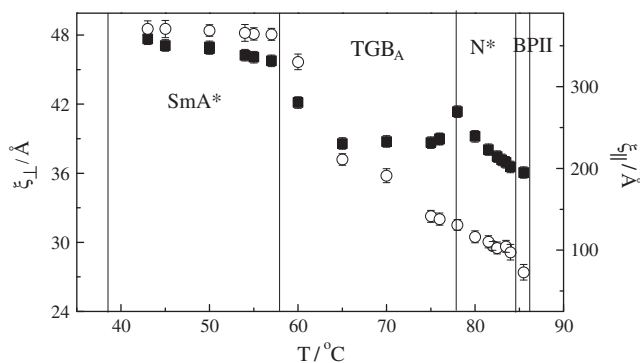


Fig. 11. Temperature dependence of the longitudinal, ξ_{\parallel} (open circles) and the transverse, ξ_{\perp} (close squares) correlation lengths within the mesophases.

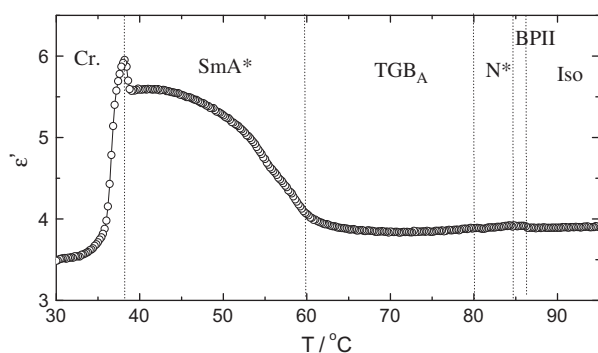


Fig. 12. Temperature dependence of the real part of complex permittivity measured on cooling at a frequency of 160 Hz.

is evidently higher than that for the material studied in the present work; the difference is more than 40 K [28].

4. Summary of the results and conclusions

The mesomorphic and structural properties of a liquid crystalline material with chiral lactate group possessing a blue phase, cholesteric, TGB_A and SmA^* phases has been studied by different experimental techniques.

The layer spacing (d) in the SmA^* phase, determined from X-ray diffraction measurements, is slightly temperature dependent. Within the TGB_A phase, the d/l ratio indicates the existence of monolayer SmA blocks and identifies the TGB phase of this compound to be composed of blocks of SmA layers.

Definite discontinuities in the X-ray scattering are observed at the N^*-TGB_A phase boundary. The increased intensities at this phase transition mark the onset of the long range smectic ordering of the TGB_A phase. A rapid increase in the X-ray scattering intensities is again observed at the TGB_A-SmA^* phase transition, perhaps due to the presence of strong Smectic A^* fluctuations. Since, the transition from the N^* phase to the SmA^* phase in this compound is facilitated *via* the formation of the TGB_A phase, both the appearance of the smectic blocks at the N^*-TGB_A phase transition as well as the disappearance of the helical twist of the cholesteric director at the TGB_A-SmA^* phase boundary is clearly reflected from the

temperature dependence of the scattered X-ray intensities. Similar behaviour is also observed in the d values obtained for this compound.

The in-plane transverse correlation length ξ_{\perp} as well as the longitudinal correlation length ξ_{\parallel} are found to be much higher for higher ordered phase than those for the lower order phase. The ξ_{\perp} values diverge near the TGB_A-N^* phase transition indicating second order phase transition.

Acknowledgements

This work is supported by Projects: GA ASCR IAA100100911, CSF P204/11/0723, RFA51 02.740.11.5166 and CSF 202/09/0047. We would like to express our gratitude to Dr. U. Baumeister for access to the 2D area X-ray detector that allows us to record the diffraction patterns. We are also very thankful to Dr. M. Prehm for assistance in recording the X-ray diffraction images.

References

- [1] J.P.F. Lagerwall, F. Giesselmann, *ChemPhysChem* 7 (2006) 20.
- [2] P. de Gennes, J. Prost, *The Physics of Liquid Crystals*, Clarendon Press, Oxford, 1999.
- [3] S.T. Lagerwall, *Ferroelectric and Antiferroelectric Liquid Crystals*, Wiley-VCH Verlag GmbH, Weinheim, 1999.
- [4] H. Taniguchi, M. Ozaki, K. Yoshino, K. Satoh, N. Yamasaki, *Ferroelectrics* 77 (1988) 137.
- [5] S.A. Pakhomov, M. Kašpar, V. Hamplová, A.M. Bubnov, H. Sverenyák, M. Glogarová, I. Stibor, *Ferroelectrics* 212 (1998) 341.
- [6] A. Bubnov, V. Hamplová, M. Kašpar, M. Glogarová, P. Vank, *Ferroelectrics* 243 (2000) 27.
- [7] V. Hamplová, A. Bubnov, M. Kašpar, V. Novotná, M. Glogarová, *Liq. Cryst.* 30 (2003) 493.
- [8] V. Hamplová, A. Bubnov, M. Kašpar, V. Novotná, D. Pocięcha, M. Glogarová, *Liq. Cryst.* 30 (2003) 627.
- [9] V. Hamplová, A. Bubnov, M. Kašpar, V. Novotná, Y. Lhotáková, M. Glogarová, *Liq. Cryst.* 30 (2003) 1463.
- [10] M. Kašpar, A. Bubnov, V. Hamplová, S. Pirkel, M. Glogarová, *Liq. Cryst.* 31 (2004) 821.
- [11] A. Bubnov, M. Kašpar, V. Hamplová, M. Glogarová, S. Samaritani, G. Galli, G. Andersson, L. Komitov, *Liq. Cryst.* 33 (2006) 559.
- [12] D. Catalano, V. Domenici, A. Marini, C.A. Veracini, A. Bubnov, M. Glogarová, *J. Phys. Chem. B* 110 (2006) 16459.
- [13] W.-L. Tsai, S.-W. Yen, M.J. Hsie, H.-C. Lee, C.M. Fu, *Liq. Cryst.* 29 (2002) 251.
- [14] W.L. Tsai, T.Ch. Lu, H.W. Liu, M.Y. Tsai, C.M. Fu, *Liq. Cryst.* 27 (2000) 1389.
- [15] M. Kašpar, P. Bilková, A. Bubnov, V. Hamplová, V. Novotná, M. Glogarová, K. Knižek, D. Pocięcha, *Liq. Cryst.* 35 (2008) 641.
- [16] V. Novotná, V. Hamplová, A. Bubnov, M. Kašpar, M. Glogarová, N. Kapernaum, S. Bezner, F. Giesselmann, *J. Mater. Chem.* 19 (2009) 3992.
- [17] N. Podoliak, V. Novotná, M. Glogarová, V. Hamplová, M. Kašpar, A. Bubnov, N. Kapernaum, F. Giesselmann, *Phase Transitions* 83 (2010) 1026.
- [18] V. Novotná, V. Hamplová, M. Kašpar, N. Podoliak, A. Bubnov, M. Glogarová, D. Nonnenmacher, F. Giesselmann, *Liq. Cryst.* 38 (2011) 649.
- [19] A. Bubnov, V. Novotná, V. Hamplová, M. Kašpar, M. Glogarová, *J. Mol. Struct.* 892 (2008) 151.
- [20] A. Bubnov, S. Pakhomov, M. Kašpar, V. Hamplová, M. Glogarová, *Mol. Cryst. Liq. Cryst.* 328 (1999) 317.
- [21] M. Garić, A. Bubnov, V. Novotná, M. Kašpar, V. Hamplová, D.Z. Obadovic, M. Glogarová, *Liq. Cryst.* 32 (2005) 565.
- [22] G. Sarkar, M.K. Das, R. Paul, B. Das, W. Weissflog, *Phase Transitions* 82 (2009) 433.
- [23] G. Sarkar, B. Das, M.K. Das, U. Baumaister, W. Weissflog, *Mol. Cryst. Liq. Cryst.* 540 (2011) 188.
- [24] A. Chakraborty, M.K. Das, B. Das, S. Findeisen-Tandel, M.G. Tamba, U. Baumeister, H. Kresse, W. Weissflog, *Liq. Cryst.* 38 (2011) 1085.
- [25] D.S. Shankar Rao, S. Krishna Prasad, V.N. Raja, C.V. Yelamaggad, S. Anitha Nagamani, *Phys. Rev. Lett.* 87 (2001) 085504.
- [26] D.Ž. Obadović, A. Vajda, M. Garić, A. Bubnov, V. Hamplová, M. Kašpar, K. Fodor-Csorba, *J. Therm. Anal. Calorim.* 82 (2005) 519.
- [27] M. Kašpar, V. Hamplová, A. Bubnov, V. Novotná, unpublished results of the group.
- [28] M. Kašpar, V. Hamplová, S.A. Pakhomov, I. Stibor, H. Sverenyák, A.M. Bubnov, M. Glogarová, P. Vank, *Liq. Cryst.* 22 (1997) 557.